Particle & Particle Systems Characterization
www.particle-journal.com

Optical Response of Metallic Nanoparticle Heteroaggregates with Subnanometric Gaps

*Christos Tserkezis, Richard W. Taylor, Jan Beitner, Rubén Esteban, Jeremy J. Baumberg, and Javier Aizpurua**

The optical response of metallic nanoparticle heteroaggregates with well-defined, subnanometric interparticle gaps is studied both theoretically and experimentally for clusters formed by nanoparticles of different size and/or different material (Au and Ag). The optical spectra of the aggregates can be understood in terms of excitation of chain-like plasmon modes, which are associated with short and long linear chains that constitute the cluster internally. The dependence of the optical properties of the aggregates on the size of the metallic nanoparticles, the interparticle gaps, and the dielectric environment is revealed in model electromagnetic calculations. A rigid molecular linker, cucurbit[5]uril, is used to experimentally form Au heteroaggregates of different sized particles, as well as heteroaggregates of silver and gold. It is shown that in both types of heteroaggregates, the ratio of the two different nanoparticles provides a versatile and easily controllable way to tailor the dominant long-wavelength chain mode. Experimental tracing of the optical response of such heteroaggregates in time during aggregation supports the formation of long-wavelength modes, which can be attributed to excitation of long chains inside the clusters.

1. Introduction

Aggregates of metallic nanoparticles in close proximity are very attractive building blocks in nanophotonics because they produce enhanced local electromagnetic (EM) fields, highly confined in the interparticle gap (hot spot), with intensities dramatically exceeding those around the corresponding single nanoparticle units.[1–5] These unique properties lead to enhanced Raman scattering[2,6] and fluorescence,[7] thus making clusters[8,9] or arrays[10,11] of metallic nanoparticles ideal for spectroscopy and sensing applications. Moreover, it has been shown that large optical forces, which may trap atoms or molecules in the interparticle gap, can be generated.[12] Additionally, such systems trigger nonlinear phenomena[13] and are characterized by increased sensitivity to the local environment.[14] Finally, dimers or small clusters of metallic nanoparticles are also used as plasmonic nanometric rulers,[15] while the in-gap field localization has been exploited in nanophotonics, in the design of subwavelength optical waveguides.[16]

Interaction between metallic nanoparticles in an aggregate is controlled to a great extent by the size of the interparticle gap. Therefore, a method to obtain metallic nanoparticle clusters with well-defined, reproducible gaps is highly desirable. While good control of distances in general can be achieved for large gaps (>10 nm) with lithographic techniques,[4,17] fabricating subnanometric gaps can be particularly challenging. Self-assembly provides a much easier, cost-efficient means to achieve such small interparticle distances. However, colloid aggregates often suffer from poor reproducibility of the gaps, and a series of linking molecules, such as DNA,[18] biotin-streptavidin,[19] or multivalent thiols,[20] have been used. In reality, such rigid linkers restrict access to the EM hot spots, while the size of the interparticle gaps is still not very accurately defined. A class of molecules that have been proven efficient in providing well-controlled subnanometric gaps are cucurbit[*n*]urils (CB[*n*]s).[21,22] These are rigid, barrel-shaped macrocyclic molecules, which bind to the metallic surface through the carbonyl groups at the portals,[23] thus fixing the separation of metallic nanoparticles at precisely 0.9 nm. In addition, the internal cavity within the CB[*n*] can act as a host, allowing the placing of a target molecule at the exact center of the linked interparticle gap, where the highest field intensity is typically produced.

The far- and near-field optical properties of 3D CB[*n*]-linked assemblies of gold nanoparticles were recently studied theoretically by means of rigorous full-electrodynamic calculations,[24] and very good agreement with optical experimental characterization was obtained.[21] It was shown that the optical response of such aggregates can be interpreted in terms of excitation of modes associated with i) short and ii) long linear and quasi-linear chains that extend within the 3D clusters, which are resonant at different wavelengths. Moreover, it has been shown that the long-wavelength far-field properties of such clusters

Dr. C. Tserkezis, Dr. R. Esteban, Dr. J. Aizpurua
Donostia International Physics Center (DIPC)
and Centro de Física de
Materiales (CFM) CSIC-UPV/EHU
Paseo Manuel de Lardizabal 5
Donostia-San Sebastián 20018, Spain
E-mail: aizpurua@ehu.es
Dr. R. W. Taylor, J. Beitner, Prof. J. J. Baumberg
NanoPhotonics Centre
Cavendish Laboratory
University of Cambridge
Cambridge CB3 0HE, UK

DOI: 10.1002/ppsc.201300287

can be well reproduced by an effective optical model, in which the dominant linear chains are described by means of a macroscopic effective dipole model.[25]

Here, we present a detailed study of the dependence of the optical response of metallic nanoparticle chains and clusters on the different parameters that govern their morphology. We first study the role of parameters that are fixed in a typical experimental realization of the clusters due to the use of the rigid CB[*n*] linkers, such as the dielectric environment and the interparticle gap itself. We then introduce new degrees of freedom in the design of plasmonic aggregates by mixing metallic nanoparticles of different sizes, as well as particles made of different materials, and explore the tunability possibilities offered by such size- and material-heteroaggregates. We focus particularly on gold–silver (Au–Ag) heteroaggregates, which are not yet completely understood. First, we explain the origin of the most prominent features in the spectra of linear chains of different size. We then study more complex, disordered chains and large, dendritic-like 3D clusters, which we compare to the corresponding gold clusters in order to identify whether the modal analysis based on chains within the cluster applies also to the case of heteroaggregates.

2. Chains of Identical Gold Nanoparticles

We begin by considering linear chains of gold spherical nanoparticles with radius a = 20 nm, separated by the 0.9-nm-wide gaps defined by CB[*n*]s, in water (for which we assume a dielectric constant ε = 1.77), illuminated by a plane wave with electric field amplitude E_0, and polarized along the chain axis. This particular particle size will be used in most of the paper for reasons that will become clear later. In **Figure 1**a, we present the wavelength (λ) dependence of the extinction cross section, σ_{ext}, normalized to the geometrical cross section obtained as $N\pi a^2$, where N is the number of particles in a chain, for linear chains consisting of 2–16 nanoparticles, as shown schematically in the figure. Similar chains have been recently studied by others as well.[9,26] The spectra of field enhancement at the gap for the same number of particles are shown in Figure 1b. As the number of nanoparticles increases, the long-wavelength, dipole-like chain mode originating from the interaction among the dipole plasmon modes of all the nanoparticles that constitute the chain gradually redshifts.[21,24] The electric field enhancement distribution around the particles for this low-energy mode in chains of two, four, eight, and 16 particles, shown in Figure 1d, indeed demonstrates the build-up of the whole dipole built from the interacting ensemble of gap plasmon modes. For chains consisting of about 12–16 nanoparticles, the resonance shift of this mode saturates, and its wavelength remains almost constant, at $\lambda_{res} \approx$ 820 nm, as shown in Figure 1c. For example, the difference in λ_{res} between a 15- and a 16-nanoparticle chain is less than 2 nm. For this reason, in what follows we will be focusing our analysis on chains built of 16 nanoparticles, for which it can be assumed that saturation of the long-chain modes has occurred. Interestingly, the largest normalized extinction cross section, and the maximum electric field enhancement at a gap, E_{max}/E_0, are obtained for shorter chains, consisting of four to six nanoparticles, as observed in Figure 1b. We should note here that, throughout the paper, by E_{max} we refer to the value of the electric field at the middle of the gap for which the largest field is obtained in each case. Higher-energy modes, which have been studied in detail and are described as bright sub-radiant modes,[27] appear as shoulders in the extinction cross sections of longer chains, and manifest themselves more clearly in the spectra showing the maximum near-field enhancement. On the other hand, the mode at about 540 nm, which remains almost independent of the chain length, presents a much smaller near-field enhancement and can be understood as a hybridized mode originating from the interaction between higher-order modes of the individual gold nanoparticles. This hybridization is possible due to the very strong interaction between the particles at these small particle separations.[28]

Before exploring potential ways to tailor the optical response of chains of metallic nanoparticles by introducing additional degrees of freedom, it is useful to examine the effect of modifying the parameters that are fixed in the synthesis of CB[*n*]-assisted self-assemblies, i.e., the interparticle gap and, to a lesser extent, the dielectric constant (ε_{env}) of the environment.

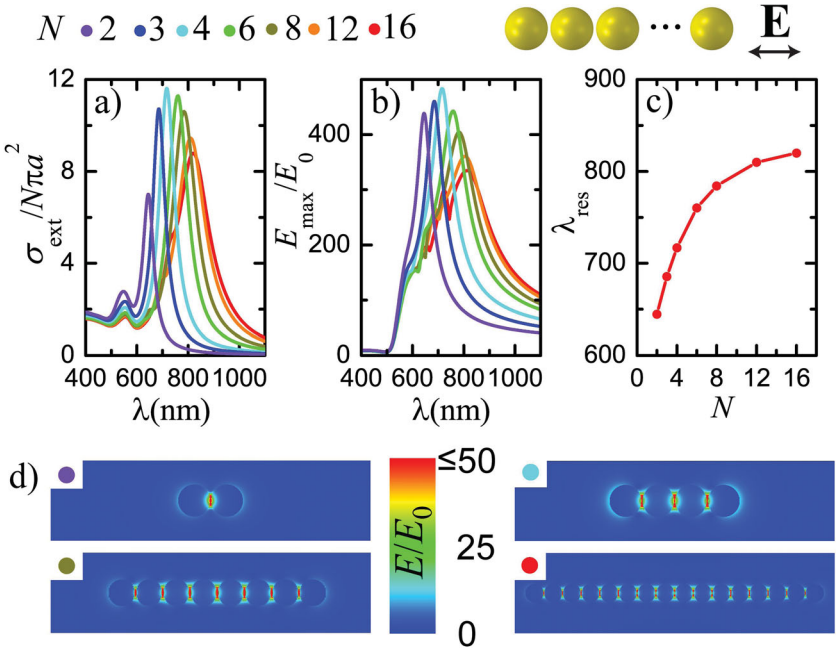

Figure 1. a) Normalized extinction cross section and b) maximum field enhancement at the gaps, for linear chains of N gold spherical nanoparticles (shown schematically on top) with radius a = 20 nm, separated by 0.9-nm-wide gaps, in water, calculated for incident light polarized along the chain axis. c) Dependence of the chain-mode wavelength, λ_{res}, on the number of particles comprising the chain. d) Electric field enhancement for chains consisting of two, four, eight, and 16 nanoparticles, at the chain-mode wavelength for each case (λ_{res} = 644, 716, 784, and 820 nm, respectively).

DOI: 10.1002/ppsc.201300287

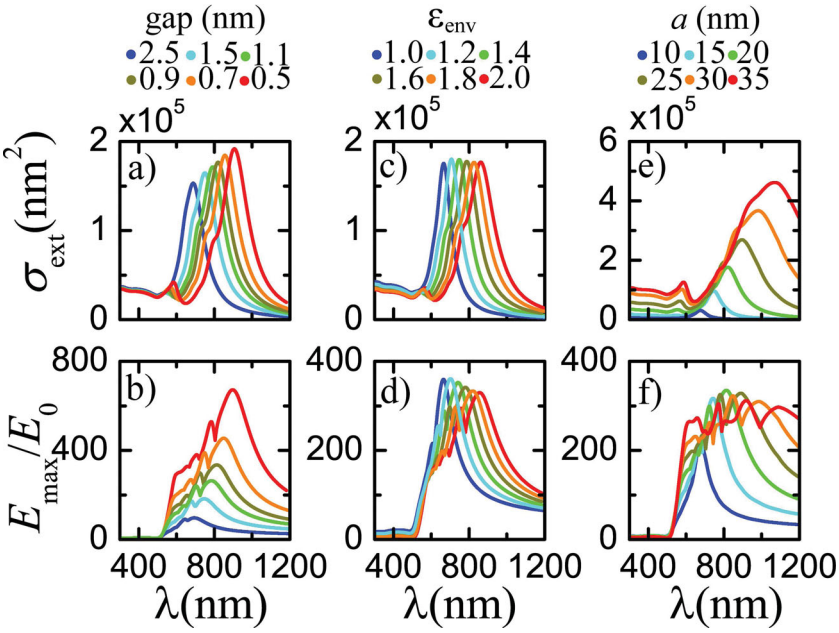

Figure 2. a) Extinction cross sections and b) maximum field enhancement for linear chains consisting of 16 gold spherical nanoparticles (a = 20 nm), in water, calculated for interparticle gaps decreasing from 2.5 to 0.5 nm. c) Extinction cross sections and d) maximum field enhancement for linear chains consisting of 16 gold nanoparticles (a = 20 nm), with interparticle gaps equal to 0.9 nm, in dielectric environments with $1 \leq \varepsilon_{env} \leq 2$. e) Extinction cross sections and f) maximum field enhancement for linear chains consisting of 16 gold nanoparticles with radii increasing from 10 to 35 nm by steps of 5 nm, separated by 0.9-nm-wide gaps, in water. In all cases, the incident plane wave is polarized along the chain axis.

In **Figure 2**a,b, we present extinction spectra and maximum near-field enhancements, respectively, for linear chains consisting of 16 gold nanoparticles with radius a = 20 nm and interparticle gaps decreasing from 2.5 to 0.5 nm (which is about the smallest gap that can be treated within classical EM theory without quantum mechanical effects becoming relevant.[29,30] Clearly, the chain mode undergoes large redshifts, of more than 200 nm, as the nanoparticles are brought closer to each other (Figure 2a), while the maximum field enhancement at a gap (the gap for which the largest field value is obtained in each case) becomes nearly 10 times larger (Figure 2b). This behavior stresses the importance of having control of the interparticle gaps in plasmonic clusters, as provided here for instance by the CB[n]s.

Another factor that can be significant in defining the optical response of metallic nanoparticle aggregates is the dielectric environment, as shown in the extinction spectra of Figure 2c for different values of ε_{env}. For example, preparing such aggregates in aqueous solutions and then drop-casting them could lead to strong blueshifts of the modes. Modification of the dielectric constant of the ambient medium from values of 1–2 leads to a redshift of the chain mode of the order of 200 nm, about twice as large as that in the case of a gold nanoparticle dimer, thus demonstrating the increased refractive index sensitivity provided by nanoparticle chains. It is also worth noting that modifying the dielectric constant of the ambient medium does not significantly affect the maximum near-field enhancement, as shown in Figure 2d.

One of the most straightforward steps that one could take in order to tune the optical response of any metallic nanostructure would be simply employing nanoparticles of different sizes. The dependence of the plasmon resonances of gold nanoparticles on size has been studied extensively,[31] and it is well known that the optical response shifts to longer wavelengths as the particle radius increases. In our chains of strongly interacting metallic particles, the plasmon modes of the individual particles form long-chain modes, which broaden and redshift drastically as the size of the particles increases, as shown in Figure 2e for chains consisting of 16 nanoparticles with radii ranging between 10 and 35 nm. However, for these long chains, the largest field enhancement (shown in Figure 2f) is obtained for particles of radius 15–25 nm. For this reason, throughout the rest of the paper, we will mostly consider clusters built of nanoparticles of radii equal to 20 nm.

3. Heteroaggregates of Different Particle Sizes

Once the dependence of the modes with particle size has been discussed, it is interesting to examine heteroaggregates composed of particles of different sizes. We will focus on the specific case of mixing gold spherical nanoparticles of two different radii, 20 and 10 nm. In order to understand how the modes in such aggregates evolve, we will use as a starting point the linear 16-nanoparticle chain studied in Section 2 and gradually substitute some of the 20-nm (large) particles with 10-nm (small) ones. The calculated extinction spectra are shown in **Figure 3**a, with the exact size distribution in the heteroaggregates shown to the right of the figure. As the number of small particles increases, the dominant chain mode blueshifts, while higher-order modes become less and less discernible, as expected. This blueshift indicates that the nanoparticle chains behave as effectively shorter dipoles, though ascribing an effective length to a chain is not straightforward, since the chains do not behave as typical optical half-wave antennas. We note that the dipole plasmon resonance of a 10-nm gold particle in water is at 521 nm, while for a 20-nm particle it is at 524 nm. The shift of a 16-particle chain, on the other hand, as we gradually proceed from a case composed only of small particles (blue curve) to a case containing only large particles (red curve), is approximately 150 nm, highlighting the collective character of the chain modes.

In Figure 3b, we present the corresponding near-field spectra. It can be seen that, in all of the cases, very large electric field enhancements are obtained at the gaps, regardless of the ratio of small-to-large particles in each case. It is therefore interesting to examine the effect of the order of small and large particles in a chain on its far- and near-field properties. This is

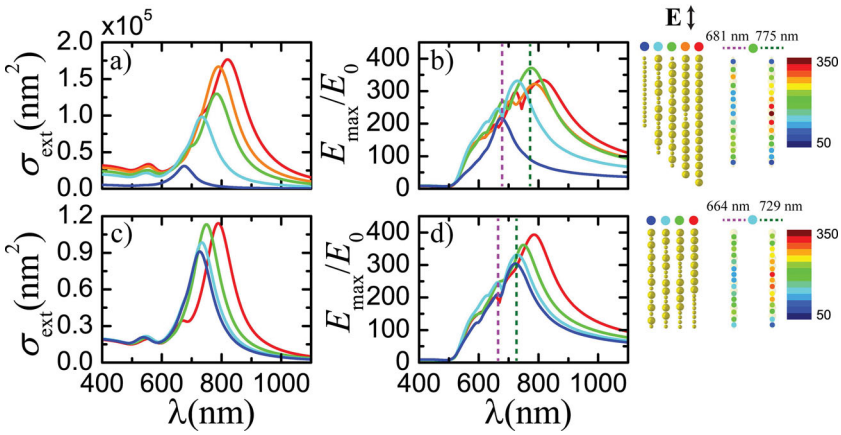

Figure 3. a) Extinction cross sections and b) maximum field enhancement for 16-particle linear chains consisting of gold spherical nanoparticles with radii equal to 20 nm (large) and 10 nm (small), calculated for varying ratios of small to large particles, as shown schematically on the right-hand side. Next to the schematics, we represent the near-field enhancement with a color code at every gap for a specific chain configuration, the one marked with the green dot, at the two wavelengths (681 and 775 nm) marked in b) by the vertical dashed lines. c) Extinction cross sections and d) maximum field enhancements for 16-particle linear chains with constant ratio of small to large particles at 1:1, for the different spatial configurations of the particles shown on the right-hand side. Next to the schematics, we represent the near-field enhancement with a color code at every gap for a specific chain configuration, the one marked with the light-blue dot, at the two wavelengths (664 and 729 nm) marked in d) by the vertical dashed lines. In all graphs, the interparticle gaps are 0.9 nm wide and the incident plane wave is polarized along the chain axis.

done in Figure 3c,d, where we keep the ratio of small-to-large particles constant at 1:1 and modify their arrangement inside the chain. When large and small individual particles or dimers are alternated in the chain, both the extinction spectra shown in Figure 3c and the near-field spectra of Figure 3d remain nearly identical (blue and green curves). On the other hand, when larger contiguous blocks of particles of equal sizes can be found within the chain (red curve), differences in the extinction spectra become more pronounced, and larger maximum field enhancements are obtained. Most notably, when the 16-particle chain consists of a sequence of two smaller chains, one made of 10-nm particles and one made of 20-nm particles, two discrete peaks are discernible in the extinction spectrum. These peaks can be associated with the chain-modes of the two constituent smaller chains: the first peak appears at 665 nm, close to the chain resonance of a chain consisting of eight 10-nm particles, and the second at 785 nm, close to the chain resonance of a chain consisting of eight 20-nm particles. The larger electric fields obtained in these cases can be understood by the presence of larger blocks, consisting of four to eight 20-nm particles, which, as already discussed in Figure 1b, produce the largest field enhancements.

In order to experimentally explore the trends of the modes with varying composition of the clusters, we synthesized and studied the optical response of large CB[5]-assisted heteroaggregates composed of nanoparticles of two different sizes. We note that the synthesized aggregates are not straight chains, but can present more complex morphology. However, their optical response can be connected to that of chains by analyzing the clusters in terms of long-chain modes and localized dimer modes.[21,24] In **Figure 4**a, we show a scanning electron microscopy (SEM) image for such a heteroaggregate, formed by mixing solutions of 10- and 30-nm gold nanoparticles at a 20:1 particle number ratio. Additional details of the synthesis procedure can be found in the Experimental Section. The image verifies the well mixed nature of such heteroaggregates and confirms that the composition ratios in the aggregate are similar to those in the initial solutions. We note that the nanoparticle sizes in Figure 4a are slightly larger than in the simulations in order to better visualize the mixing of the two different components in the aggregates. In Figure 4b, we show an enlarged view of Figure 4a, which verifies that regions of

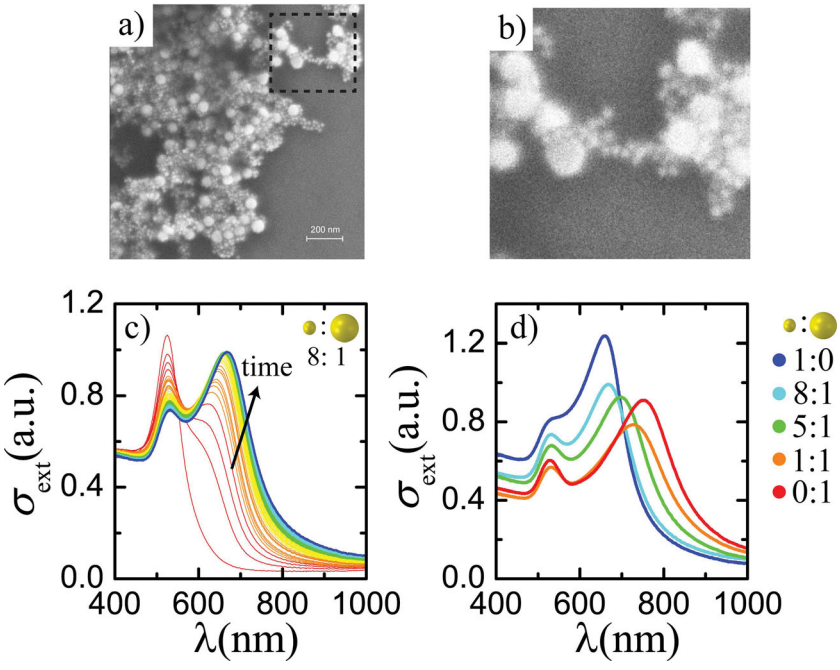

Figure 4. a) SEM image of CB[5]-assisted heteroaggregates consisting of small (a = 10 nm) and large (a = 30 nm) gold nanoparticles, mixed at a 20:1 particle number ratio respectively, and b) an enlarged view of Figure 4a in the region marked by the box. c) Time resolved extinction spectra experimentally obtained for a CB[5]-assisted aggregation of small (a = 10 nm) and large (a = 20 nm) gold nanoparticles (with small-to-large particle ratio equal to 8:1) in water. The spectra are acquired at 10 s intervals for 10 min. d) Experimental extinction spectra of heteroaggregates of CB[5]-linked small and large gold nanoparticles in water, for the small-to-large particle ratios shown on the right-hand side.

Part. Part. Syst. Charact. **2013**,
DOI: 10.1002/ppsc.201300287

mixed nanoparticle chains can be identified within the clusters.

Experimental extinction spectra obtained during aggregation of a cluster comprising 10- and 20-nm gold particles mixed at a ratio of 8:1 respectively (to provide matched collision cross sections that build mixed aggregates) are presented in Figure 4c. Clearly, over time, the plasmon resonance associated with the individual nanoparticles rapidly decreases and broadens, while a second broad resonance, arising from aggregation, appears and gradually redshifts. This resonance resembles strongly the corresponding long-wavelength resonance in gold homoaggregates studied in Taylor et al.,[21] supporting the assumption of the excitation of chain modes that comprise both types of nanoparticles in the chain. This behavior is consistent with the response found for the linear chains of particles of two different sizes studied in Figure 3a,c. In Figure 4d, we present the experimental extinction spectra for clusters created with different proportion of small-to-large particles, ranging from 0:1 to 1:0. Similarly to the case of linear chains shown in Figure 3a, the long-wavelength chain mode undergoes a blueshift of more than 100 nm as the number of small particles increases, which practically implies that the position of the long-chain mode can be easily controlled by the ratio of the two particle sizes mixed to synthesize the aggregate. We should also note here that the different extinction spectra shown in Figure 4d are obtained for solutions containing different total numbers of particles, which explains why larger extinction values are obtained for clusters with greater small-to-large particle ratios.

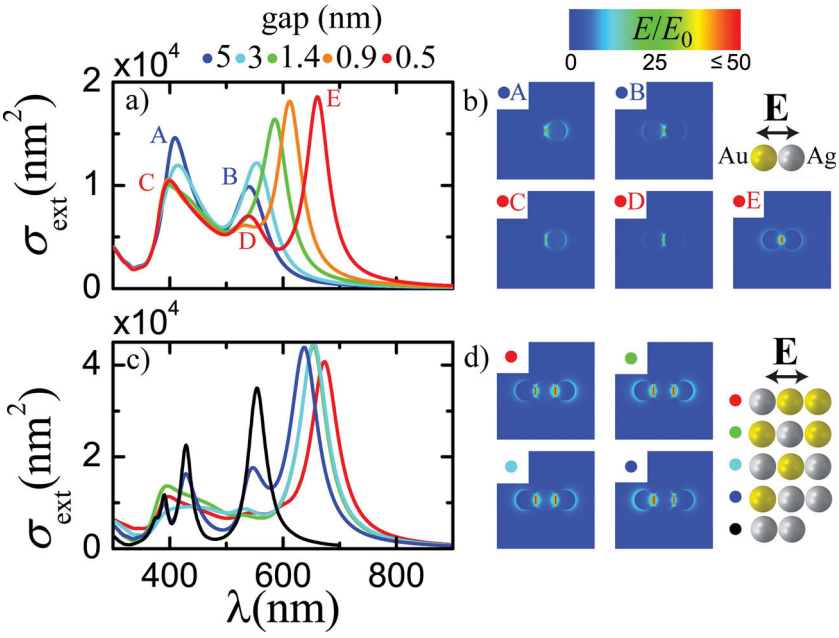

Figure 5. a) Extinction cross sections calculated for Au–Ag dimers with gaps equal to 5, 3, 1.4, 0.9, and 0.5 nm. b) Near-field plots at the resonances of the 5-nm-gap (upper plots) and the 0.5-nm-gap (lower plots) cases. The wavelength of each field plot is denoted by a capital letter (A, B, C, D, E) mapping each resonance in the corresponding extinction spectrum in a). c) Extinction cross sections for the Au–Ag trimers shown schematically on the right-hand side (with gaps equal to 0.9 nm), and d) near-field plots corresponding to the longer wavelength resonance in each case. In all graphs, the particles have a radius of 20 nm, the ambient medium is water, and the incident plane wave is polarized along the dimer/trimer axis.

4. Heteroaggragates of Gold and Silver Nanoparticles

So far, we have studied clusters consisting exclusively of gold nanoparticles, and explored the possibility of tuning their optical response by modifying the geometrical properties (gaps and size) and the dielectric environment of the clusters. Most of these parameters, however, are usually well defined in the CB[*n*]-assisted self-assembly procedure, and provide moderate aprioristic flexibility. We will now focus on Au–Ag heteroaggregates, and show how the admixture of two different materials offers an easy alternative way to control the wavelength of the modes. Au–Ag heteroaggregates have attracted less interest compared to homogeneous aggregates, with most of the studies being limited only to dimers.[32–34] In **Figure 5**a, we show how the extinction spectra of Au–Ag dimers in water evolve as the interparticle gap decreases, when the incident light is polarized along the dimer's axis. For relatively large separations (larger than 2–3 nm), the two resonances at about 410 nm and 545 nm can be identified as originating from the individual silver and gold nanoparticles, respectively (see for example resonances A and B in Figure 5a for the case of a 5-nm-wide gap). They are hybridized modes, but they shift only slightly in wavelength with respect to the corresponding resonances of the individual particles.[32] The modal patterns can be verified by the corresponding electric field distributions shown in Figure 5b for each resonance, where it is clearly shown that the field is more localized around one of the two particles, either the silver particle (plot A of Figure 5b) or the gold one (plot B in Figure 5b), depending on the wavelength. As the interparticle gap becomes smaller, the interaction between the two nanoparticles becomes stronger, leading to a large redshift and increased strength of the bonding dipole mode, and the electric field is now more smoothly distributed around the whole dimer (mode E in Figure 5a,b).[29,35] In addition, a hybridized quadrupole-like mode evolves at about 540 nm (D), and its position remains almost unaffected by the width of the gap. Finally, the broad peak at about 410 nm (C) has been described as a Fano resonance originating from the interaction between the sharp hybridized antibonding mode of the dimer, close to the resonance of a single Ag particle, and the continuum of the Au interband transitions.[32] It is worth noting that, while at first this mode redshifts as the gap width decreases, from 409 nm for a 5-nm-wide gap to 415 nm for a 3-nm-wide gap (blue and light blue lines in Figure 5a, respectively), for even smaller gaps (and thus stronger interactions) it finally starts to blueshift, to about 400 nm for the 0.5-nm-wide gap (red line in Figure 5a).

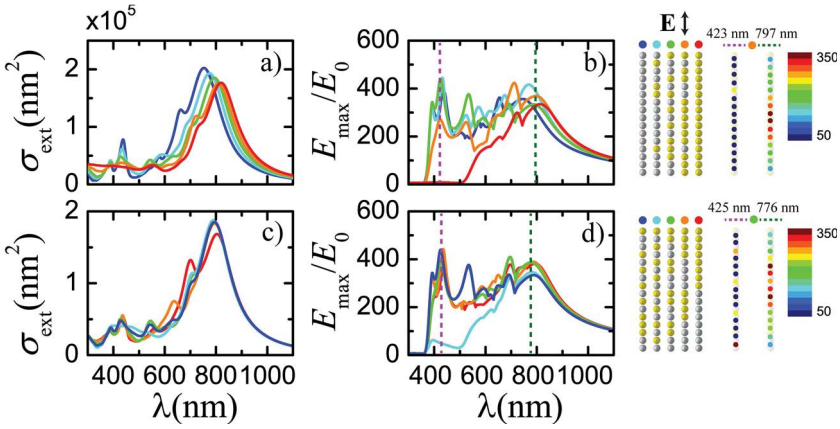

Figure 6. a) Extinction cross sections and b) maximum near-field enhancement calculated for Au–Ag nanoparticle chains with different Au:Ag ratios, as shown schematically on the right-hand side. Next to the schematics, we represent the near-field enhancement with a color code at every gap for a specific chain configuration, the one marked with the orange dot, at the two wavelengths (423 and 797 nm) marked in b) by the vertical dashed lines. c) Extinction cross sections and d) maximum near-field enhancements for the different arrangements of Au–Ag clusters (Au:Ag ratio equal to 1:1) shown on the right-hand side. Next to the schematics, we represent the near-field enhancement with a color code at every gap for a specific chain configuration, the one marked with the green dot, at the two wavelengths (425 and 776 nm) marked in b) by the vertical dashed lines. In all graphs, the chains consist of 16 nanoparticles with radius a = 20 nm and interparticle gaps equal to 0.9 nm, in water, and the incident plane wave is polarized along the chain axis.

To analyze the evolution of the optical response in material heteroaggregates as a function of the number of particles, we add a third particle to the dimer structures under consideration. In Figure 5c, we show the extinction spectra for all the possible arrangements in a linear trimer of gold and silver particles with gaps equal to 0.9 nm. Silver nanoparticle trimers with more complex spatial configurations (e.g., triangles) were recently studied in relation to their enhanced Raman scattering and optical activity.[36] When two particles of the same material are placed next to each other, the extinction spectrum retains many of the characteristics of the corresponding dimer, with some additional peaks due to the presence of the third particle and its interaction with that dimer. This is better demonstrated in Figure 5c in the case of a trimer containing two neighboring silver particles, where all of the resonances of a silver dimer (black line) are reproduced in the extinction spectrum of the trimer (blue line). On the other hand, interestingly, when gold and silver particles in the trimer appear with alternating order, the position, strength, and lineshape of the long-wavelength bonding dipole mode remain very stable, regardless of whether the trimer contains two gold or two silver particles, and the differences in their extinction spectra (green and light blue line in Figure 5c) are practically indiscernible. This indicates that in the long-wavelength regime the type of metallic material each nanoparticle is made of plays a smaller role in defining the optical response of a cluster, as can be also verified by the striking similarity of the corresponding near-field distributions calculated in Figure 5d for the longer wavelength resonance. At long enough wavelengths, both metals are very similar, Drude-like metals and the differences in their optical response become less important. For shorter wavelengths, the individual core-electron structure of the two metals prevails, higher-order modes are efficiently excited and distinguishable in the extinction spectra and their position is determined by the exact spatial configuration of the particles in the trimer.

We shall now focus on larger linear chains containing both types of material. In order to directly compare with the case of aggregates formed exclusively of gold, as those studied in Section 2, we show in **Figure 6** linear chains comprising 16 nanoparticles with radii equal to 20 nm, in water. In the upper panel (Figure 6a,b), where we change the material of the particles, the ratio of Au:Ag is modified gradually from 0:1 to 1:0 in arrangements shown schematically on the right-hand side of the figure. In the lower panel, the Au:Ag ratio is kept constant at 1:1, and the relative positions of the particles within the chain are then modified. From both extinction diagrams (Figure 6a,c), it is evident that the similar, large negative values of the permittivity of the two metals prevail at longer wavelengths, in analogy to the lightning-rod effect in the infrared,[10] determining the modal position very robustly. As the number of silver nanoparticles increases, the far-field response of the chain shifts gradually towards that of a chain made exclusively of silver nanoparticles. For other intermediate ratios, the chain mode behaves as that of a linear chain of 16 metallic nanoparticles made by some metal with an intermediate plasma frequency. Moreover, it is worth noting that this mode is weakly affected by the relative positions of gold and silver nanoparticles in the aggregate. However, this is not the case for the near-field properties of the chains, where the presence of shorter silver particle blocks (and to a lesser extent gold ones) manifests itself by significant field enhancements in relatively narrow wavelength regions around 400–450 nm, as can be verified by the field schematics on the right-hand side of Figure 6. The field enhancements achieved in those cases are even larger than those associated with the broad low-energy mode (Figure 6d).

Having explored the far- and near-field optical response of linear chains of gold and silver nanoparticles, we will now study the realistic case of kinked chains, which are commonly found in self-assembled 3D clusters. In Esteban et al.,[24] it was shown that the optical response of kinked chains of gold nanoparticles is quite robust with respect to disorder in the chain, with their chain modes experiencing small blueshifts as disorder increases, until a chain with its axis parallel to the incident electric field can no longer be found in the cluster. This behavior is reproduced in the left-hand side spectra of **Figure 7**, where the optical extinction (Figure 7a) and the near-field at the gap (Figure 7c) are obtained for different disordered configurations of a chain of homoaggregates. The spectra can be compared to the extinction spectra and near-field enhancements of the corresponding Au–Ag heteroaggregates, shown in Figure 7b,d. In all of the Au–Ag chains, the ratio Au:Ag is kept constant at 1:1 and the relative positions of the individual gold and silver particles in the aggregate are also maintained, as shown in the top

Part. Part. Syst. Charact. **2013**,
DOI: 10.1002/ppsc.201300287

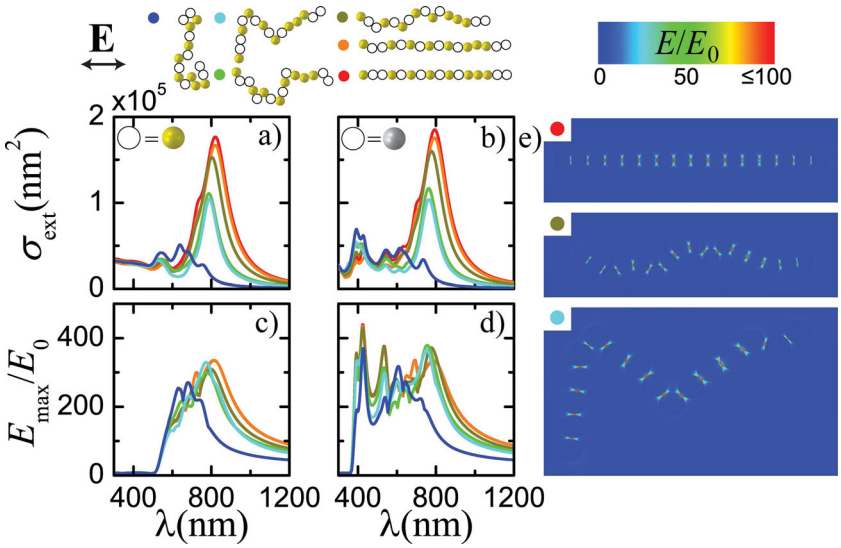

Figure 7. a,b) Extinction cross sections and c,d) maximum near-field enhancements calculated for the Au (left) and Au–Ag (right) disordered chains shown schematically on top. e) Near-field plots at the wavelength of the chain mode for three of the Au–Ag chains under study. In all graphs, the particles have a radius of 20 nm, the interparticle gaps are 0.9 nm wide, the ambient medium is water, and the incident light is polarized as shown schematically in the figure.

schematics of Figure 7. In the long-wavelength regime, both near- and far-field diagrams are very similar in modal shape and intensity, with the main difference being the small blueshift of the modes in the Au–Ag heteroaggregates, already expected from the results for linear chains in Figure 6. Additional extinction peaks and significant near-field enhancements appear for higher energies. These are associated mostly with the presence of silver dimers, as can be verified by their corresponding near-field distributions (not shown here). The formation of modes extending along long chains, similar to those shown in Esteban et al.,[24] as a result of gap-plasmon coupling, is better demonstrated in the near-field distributions shown in Figure 7e for three disordered configurations of Au–Ag heteroaggregates. We note that even for very disordered chains, large field enhancements, greater than 100, are obtained in all of the gaps in the chains, although, naturally, the absolute values depend on the orientation of each part of the chains with respect to the incident electric field.

In **Figure 8**, we explore the effect of varying the ratio of Au:Ag in more realistic, disordered 3D heteroaggregates. We calculate the response of clusters consisting of thirty 20-nm nanoparticles, modifying gradually the Au:Ag ratio from 0:1 to 1:0. The exact geometry of the clusters is shown on the right-hand side of the figure. This geometry is fixed in all cases, and only the material of the constituent nanoparticles is modified according to the ratio desired. The spectra are vertically shifted for clarity. As the Au:Ag ratio changes, the modes show a behavior similar to that of the linear chains studied in Figure 6: the main, long-wavelength mode redshifts as the number of Au nanoparticles in the cluster increases, while modes around 400 nm progressively appear as the number of Ag nanoparticles increases. Many additional extinction peaks can also be observed at intermediate wavelengths. These peaks can be associated with the excitation of shorter chains within the clusters. As the cluster size increases, more chains with similar resonance wavelengths are expected to be excited, smoothing the spectra, with fewer, broader peaks.

Finally, in **Figure 9**, we experimentally study the optical response of large 3D CB[5]-assisted Au–Ag self-assemblies. In Figure 9a, we present a SEM image of Au–Ag heteroaggregates, which confirms the formation of dendritic-like clusters containing long, almost linear chains of nanoparticles. We note that the nanoparticles in Figure 9a have a radius equal to 30 nm in order to appreciate better the position of the particles within the cluster. While we believe that the mixing of the two components is very good (see Experimental Section), it is difficult to distinguish Au and Ag, as can be also verified by transmission electron microscopy (TEM) images obtained during aggregation, as shown in Figure 9b.

In Figure 9c, we show experimental time-resolved extinction spectra for a specific Au:Ag ratio, 15:1. Initially, two extinction peaks, at about 405 and 525 nm, associated with the individual silver and gold nanoparticles, respectively, can be observed. As time elapses and aggregation proceeds, these two extinction peaks become less pronounced, while a broad resonance at longer wavelengths is formed. In view of our previous discussion about the similarity of the two metallic materials in the long-wavelength regime, this resonance can be directly attributed to the excitation of long Au–Ag chains, supporting the validity of the chain modal analysis also for the case of heteroaggregates of two different materials. In Figure 9d, we explore the effect of modifying the Au:Ag ratio in an experiment of 3D self-assembled heteroaggregates. Clearly, the low-energy mode undergoes large blueshifts, of the order of 150 nm, as the Au:Ag ratio is gradually modified from 1:0 to 0:1. Such shifts are in good agreement with those obtained theoretically in Figure 8, and consistent with the tendencies found for the

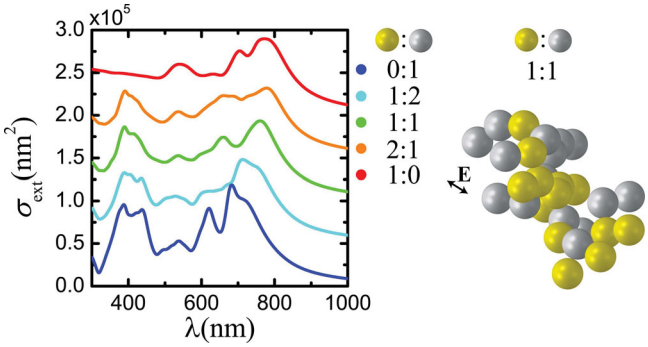

Figure 8. Extinction spectra for 3D Au–Ag heteroaggregates consisting of a total number of 30 nanoparticles (a = 20 nm), in water, for the Au:Ag ratios shown to the right of the spectra. Extinction spectra are shifted by 5 × 10^4 nm^2 for clarity. On the right-hand side, we show the exact geometry of the Au:Ag heteroaggregates used in these calculations. The specific case of Au:Ag ratio equal to 1:1 is shown.

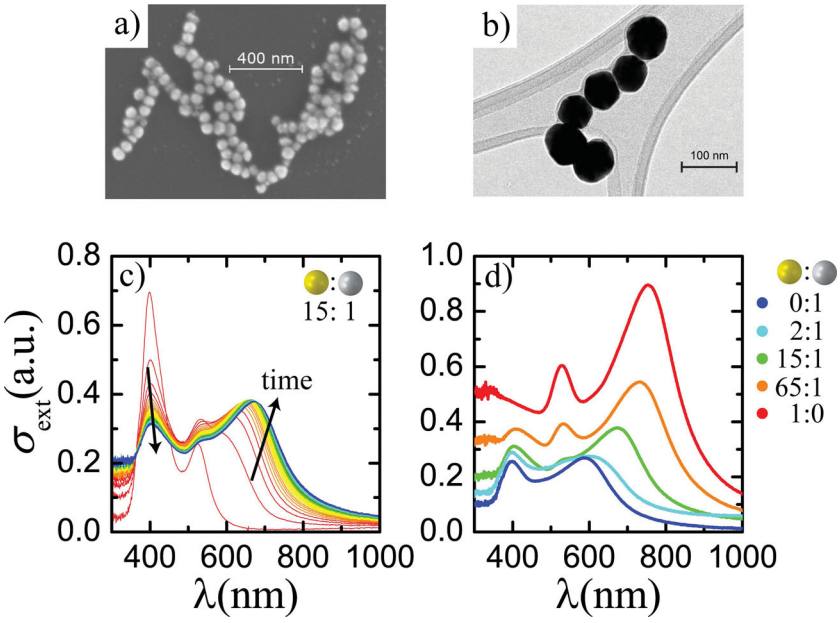

Figure 9. a) SEM image of CB[5]-assisted Au–Ag heteroaggregates (a = 30 nm) and b) a TEM image obtained during aggregation. c) Time-resolved extinction spectra experimentally obtained for CB[5]-assisted aggregation of Au–Ag nanoparticle (a = 20 nm) clusters (Au:Ag ratio equal to 15:1) in water. The spectra are acquired at 10 s intervals for 10 min. d) Experimental extinction spectra of CB[5]-linked Au–Ag nanoparticle aggregates in water, for the Au:Ag ratios shown on the right-hand side.

simpler case of linear chains studied in Figure 6a. This indicates that a simple variation of the Au:Ag ratio, which is easily controlled in the laboratory, indeed provides the ability to tune the chain modes at will. Such modes are mixed modes combining the Drude response of the constituent metals with an effective metamaterial response directing the plasmonic chain modes.

5. Conclusions

We have presented a detailed computational and experimental study of straight and disordered chains and 3D clusters of metallic nanoparticles with fixed interparticle gaps, and analyzed the dependence of their optical response on the geometrical parameters and materials making the cluster. In particular, we have shown that the wavelengths of the chain modes for such clusters depend strongly on the nanoparticle size, distance, and dielectric environment, highlighting the significance of having a way to keep these parameters fixed in a self-assembly procedure utilizing wet chemistry. We have also studied two-component heteroaggregates of different nanoparticle sizes or materials and showed that the ratio of the two components provides a versatile pathway for tuning the long-wavelength chain modes. We discussed the physical origin of the modes appearing in small Au–Ag clusters, such as dimers and trimers, where the strong interaction due to the subnanometric gaps, and the different relative positions of the particles, may lead to excitation of additional higher-energy modes. Finally, we discussed the validity of the modal analysis of large clusters in terms of chains within the cluster for the case of heteroaggregates. Most notably, we showed that in the case of Au–Ag heteroaggregates such an analysis is possible because in the long-wavelength regime, where the chain modes appear, both metals behave very similarly, like good Drude-like metals. On the other hand, for shorter wavelengths, the individual plasmonic characteristics of the two metals lead to much richer spectra, compared to the corresponding homoaggregates. Our theoretical results are supported by experiments of the optical response of heteroaggregates formed by particles of different size and material, thus introducing new possibilities to tailor the optical response of complex optical networks.

6. Experimental Section

Calculations: All of the theoretical results are obtained by rigorous, full-electrodynamic numerical simulations using the Multiple Multipole Method OpenMaX.[37] For the dielectric function of gold and silver, we use the experimental data from Johnson and Christy,[38] size-corrected according to:[39]

$$\varepsilon(\omega) = \varepsilon_{JC}(\omega) - \frac{\omega_p^2}{\omega(\omega+i\gamma_c)} + \frac{\omega_p^2}{\omega(\omega+i\gamma_p)}, \quad (1)$$

where ω is the angular frequency, ε_{JC} is the experimentally measured values of the dielectric function, ω_p is the plasma frequency of the metal, and γ_p is the intrinsic damping of the conduction-band electrons, which accounts for dissipative losses. The size correction is described by an additional damping factor, $\gamma_c = \nu_F/a$ where ν_F is the Fermi velocity of the metal and a the radius of the particles. We use ω_p = 9.056 eV, γ_p = 0.0708 eV for gold, and ω_p = 9.14 eV, γ_p = 0.0206 eV for silver, values obtained by fitting the experimental values of Johnson and Christy[38] to the Drude model, and take $\nu_F = 1.4 \times 10^6$ m s^{-1} and $\nu_F = 1.39 \times 10^6$ m s^{-1} for gold and silver, respectively.[40]

Experimental Methods: CB[5] was fabricated using the methods described in Lee and Scherman.[41] Gold and silver nanoparticles were purchased from British Biocell International and used as supplied, where nanoparticle sizes correspond to nominal diameters reported from the manufacturer. The nanoparticle ratios quoted in text for the bidisperse heteroaggregates correspond to appropriately diluted nanoparticle solutions which, when combined, give a total mixed volume of 1 mL. The nanoparticle concentrations used to determine the particle ratios are additionally quoted from the manufacturer. In all cases, the unaggregated heteronanoparticle solution was sonicated (≈5 min) to ensure good particle mixing. Aggregation of the nanoparticle solution was induced with an aliquot (≈10 µL) of CB[5] solution within measurement cuvette. CB[5] was dissolved in MilliQ water to produce an aqueous solution at 1×10^{-3} M concentration and sonicated. The concentration of CB[5] for the given nanoparticle volumes ensured that the aggregation kinetics were in the diffusion-limited regime.[21]

Extinction spectroscopy was performed in real time during the aggregation phase. Extinction spectra were recorded with an Ocean Optics spectrometer with a 3 ms integration time.

Acknowledgements

We strongly appreciate Prof. Oren Scherman for his constant support and fruitful discussions. We acknowledge funding from ETORTEK project

"nanoiker" from the Department of Industry of the Government of the Basque Country, Ministry of Science and Education, project FIS2010–19609-C02–01, Department of Education of the Basque Government, project IT756–13 of consolidated groups of the UPV/EHU, and EPSRC EP/F059396/1, EP/G060649/1, EU NanoSci-E+ CUBiHOLE, and ERC LINASS 320503 grants.

Received: August 14, 2013
Revised: October 30, 2013
Published online:

[1] J. R. Krenn, A. Dereux, J. C. Weeber, E. Bourillot, Y. Lacroute, J. P. Goudonnet, G. Schider, W. Gotschy, A. Leitner, F. R. Aussenegg, C. Girard, *Phys. Rev. Lett.* **1999**, *82*, 2590.
[2] H. Xu, J. Aizpurua, M. Käll, P. Apell, *Phys. Rev. E* **2000**, *62*, 4318.
[3] K. Li, M. I. Stockman, D. J. Bergman, *Phys. Rev. Lett.* **2003**, *91*, 227402.
[4] a) P. Mühlschlegel, H.-J. Eisler, O. J. F. Martin, B. Hecht, D. W. Pohl, *Science* **2005**, *308*, 1607; b) D. R. Ward, F. Hüser, F. Pauly, J. C. Cuevas, D. Natelson, *Nat. Nanotechnol.* **2010**, *5*, 732.
[5] J. A. Schuller, E. S. Barnard, W. Cai, Y. C. Jun, J. S. White, M. L. Brongersma, *Nat. Mater.* **2010**, *9*, 193.
[6] a) E. C. Le Ru, P. G. Etchegoin, *Chem. Phys. Lett.* **2004**, *396*, 393; b) D.-K. Lim, K.-S. Jeon, H. M. Kim, J.-M. Nam, Y. D. Suh, *Nat. Mater.* **2010**, *9*, 60; c) D.-K. Lim, K.-S. Jeon, J.-H. Hwang, H. Kim, S. Kwon, Y. D. Suh, J.-M. Nam, *Nat. Nanotechnol.* **2011**, *6*, 452; d) P. Alonso-González, P. Albella, M. Schnell, J. Chen, F. Huth, A. García-Etxarri, F. Casanova, F. Golmar, L. Arzubiaga, L. E. Hueso, J. Aizpurua, R. Hillenbrand, *Nat. Commun.* **2012**, *3*, 684.
[7] a) J. Zhang, Y. Fu, M. H. Chowdhury, J. R. Lakowicz, *Nano Lett.* **2007**, *7*, 2101; b) J.-W. Liaw, J.-H. Chen, C.-S. Chen, M.-K. Kuo, *Opt. Express* **2009**, *17*, 13532; c) Z. Zhang, P. Yang, H. Xu, H. Zheng, *J. Appl. Phys.* **2013**, *113*, 033102.
[8] A. M. Schwartzberg, C. D. Grant, A. Wolcott, C. E. Talley, T. R. Huser, R. Bogomolni, J. Z. Zhang, *J. Phys. Chem. B* **2004**, *108*, 19191.
[9] K. L. Wustholz, A.-I. Henry, J. M. McMahon, R. G. Freeman, N. Valley, M. E. Piotti, M. J. Natan, G. C. Schatz, R. P. Van Duyne, *J. Am. Chem. Soc.* **2010**, *132*, 10903.
[10] F. Le, D. W. Brandl, Y. A. Urzhumov, H. Wang, J. Kundu, N. J. Halas, J. Aizpurua, P. Nordlander, *ACS Nano* **2008**, *2*, 707.
[11] Á. Sánchez-González, S. Corni, B. Mennucci, *J. Phys. Chem. C* **2011**, *115*, 5450.
[12] a) H. Xu, M. Käll, *Phys. Rev. Lett.* **2002**, *89*, 246802; b) A. S. Zelenina, R. Quidant, M. Nieto-Vesperinas, *Opt. Lett.* **2007**, *32*, 1156.
[13] a) M. Danckwerts, L. Novotny, *Phys. Rev. Lett.* **2007**, *98*, 026104; b) S. Kim, J. Jin, Y.-J. Kim, I.-Y. Park, Y. Kim, S.-W. Kim, *Nature* **2008**, *453*, 757; c) K. D. Ko, A. Kumar, K. H. Fung, R. Ambekar, G. L. Liu, N. X. Fang, K. C. Toussaint Jr., *Nano Lett.* **2011**, *11*, 61.
[14] a) P. K. Jain, M. A. El-Sayed, *Nano Lett.* **2008**, *8*, 4347; b) S. S. Aćimović, M. P. Kreuzer, M. U. González, R. Quidant, *ACS Nano* **2009**, *3*, 1231; c) M. Piliarik, P. Kvasnička, N. Galler, J. R. Krenn, J. Homola, *Opt. Express* **2011**, *19*, 9213.
[15] a) B. M. Reinhard, M. Siu, H. Agarwal, A. P. Alivisatos, J. Liphardt, *Nano Lett.* **2005**, *5*, 2246; b) C. Tabor, R. Murali, M. Mahmoud, M. A. El-Sayed, *J. Phys. Chem. A* **2009**, *113*, 1946; c) S.-D. Liu, M.-T. Cheng, *J. Appl. Phys.* **2010**, *108*, 034313; d) R. T. Hill, J. J. Mock, A. Hucknall, S. D. Wolter, N. M. Jokerst, D. R. Smith, A. Chilkoti, *ACS Nano* **2012**, *6*, 9237.
[16] a) M. Quinten, A. Leitner, J. R. Krenn, F. R. Aussenegg, *Opt. Lett.* **1998**, *23*, 1331; b) S. A. Maier, P. G. Kik, H. A. Atwater, S. Meltzer, E. Harel, B. E. Koel, A. A. G. Requicha, *Nat. Mater.* **2003**, *2*, 229; c) A. F. Koenderink, A. Polman, *Phys. Rev. B* **2006**, *74*, 033402; d) A. Alù, N. Engheta, *Phys. Rev. B* **2006**, *74*, 205436; e) C. Tserkezis, N. Stefanou, *J. Opt. Soc. Am B* **2012**, *29*, 827.
[17] a) H. Im, K. C. Bantz, N. C. Lindquist, C. L. Haynes, S.-H. Oh, *Nano Lett.* **2010**, *10*, 2231; b) H. Duan, H. Hu, K. Kumar, Z. Shen, J. K. W. Yang, *ACS Nano* **2011**, *5*, 7593.
[18] a) A. P. Alivisatos, K. P. Johnsson, X. Peng, T. E. Wilson, C. J. Loweth, M. P. Bruchez Jr., P. G. Schultz, *Nature* **1996**, *382*, 609; b) S. Y. Park, J.-S. Lee, D. Georganopoulou, C. A. Mirkin, G. C. Schatz, *J. Phys. Chem. B* **2006**, *110*, 12673; c) J. A. Fan, Y. He, K. Bao, C. Wu, J. Bao, N. B. Schade, V. N. Manoharan, G. Shvets, P. Nordlander, D. R. Liu, F. Capasso, *Nano Lett.* **2011**, *11*, 4859; d) S. J. Barrow, A. M. Funston, D. E. Gómez, T. J. Davis, P. Mulvaney, *Nano Lett.* **2011**, *11*, 4180.
[19] a) M. Li, K. K. W. Wong, S. Mann, *Chem. Mater.* **1999**, *11*, 23; b) K. Aslan, C. C. Luhrs, V. H Pérez-Luna, *J. Phys. Chem. B* **2004**, *108*, 15631.
[20] a) C. S. Weisbecker, M. V. Merritt, G. M. Whitesides, *Langmuir* **1996**, *12*, 3763; b) A. Hofmann, P. Schmiel, B. Stein, C. Graf, *Langmuir* **2011**, *27*, 15165.
[21] R. W. Taylor, T.-C. Lee, O. A. Scherman, R. Esteban, J. Aizpurua, F. M. Huang, J. J. Baumberg, S. Mahajan, *ACS Nano* **2011**, *5*, 3878.
[22] S. Kasera, F. Biedermann, J. J. Baumberg, O. A. Scherman, S. Mahajan, *Nano Lett.* **2012**, *12*, 5924.
[23] Q. An, G. Li, C. Tao, Y. Li, Y. Wu, W. Zhang, *Chem. Commun.* **2008**, *2008*, 1989.
[24] R. Esteban, R. W. Taylor, J. J. Baumberg, J. Aizpurua, *Langmuir* **2012**, *28*, 8881.
[25] R. W. Taylor, R. Esteban, S. Mahajan, R. Coulston, O. A. Scherman, J. Aizpurua, J. J. Baumberg, *J. Phys. Chem. C* **2012**, *116*, 25044.
[26] a) M. D. Arnold, M. G. Blaber, M. J. Ford, N. Harris, *Opt. Express* **2010**, *18*, 7528; b) S. M. Adams, S. Campione, F. Capolino, R. Ragan, *Langmuir* **2013**, *29*, 4242; c) T. Chen, M. Pourmand, A. Feizpour, B. Cushman, B. M. Reinhard, *J. Phys. Chem. Lett.* **2013**, *4*, 2147.
[27] B. Willingham, S. Link, *Opt. Express* **2011**, *19*, 6450.
[28] P. Nordlander, C. Oubre, E. Prodan, K. Li, M. I. Stockman, *Nano Lett.* **2004**, *4*, 899.
[29] I. Romero, J. Aizpurua, G. W. Bryant, F. J. García de Abajo, *Opt. Express* **2006**, *14*, 9988.
[30] K. J. Savage, M. M. Hawkeye, R. Esteban, A. G. Borisov, J. Aizpurua, J. J. Baumberg, *Nature* **2012**, *491*, 574.
[31] a) S. Link, M. A. El-Sayed, *Int. Rev. Phys. Chem.* **2000**, *19*, 409; b) M. Pelton, J. Aizpurua, G. Bryant, *Laser Photon. Rev.* **2008**, *2*, 136.
[32] a) G. Bachelier, I. Russier-Antoine, E. Benichou, C. Jonin, N. Del Fatti, F. Vallée, P.-F. Brevet, *Phys. Rev. Lett.* **2008**, *101*, 197401; b) S. Sheikholeslami, Y.-W. Jun, P. K. Jain, A. P. Alivisatos, *Nano Lett.* **2010**, *10*, 2655.
[33] E. R. Encina, E. A. Coronado, *J. Phys. Chem. C* **2010**, *114*, 16278.
[34] a) E. R. Encina, E. A. Coronado, *J. Phys. Chem. C* **2011**, *115*, 15908; b) O. Peña-Rodríguez, U. Pal, M. Campoy-Quiles, L. Rodríguez-Fernández, M. Garriga, M. I. Alonso, *J. Phys. Chem. C* **2011**, *115*, 6410; c) A. Lombardi, M. P. Grzelczak, A. Crut, P. Maioli, I. Pastoriza-Santos, L. M. Liz-Marzán, N. Del Fatti, F. Vallée, *ACS Nano* **2013**, *7*, 2522.
[35] O. Pérez-González, N. Zabala, J. Aizpurua, *New J. Phys.* **2011**, *13*, 083013.
[36] a) L. Chuntonov, G. Haran, *Nano Lett.* **2011**, *11*, 2440; b) L. Chuntonov, G. Haran, *Nano Lett.* **2013**, *13*, 1285.
[37] T. Sannomiya, J. Vörös, C. Hafner, *J. Comput. Theor. Nanosci.* **2009**, *6*, 749.
[38] P. B. Johnson, R. W. Christy, *Phys. Rev. B* **1972**, *6*, 4370.
[39] S. Berciaud, L. Cognet, P. Tamarat, B. Lounis, *Nano Lett.* **2005**, *5*, 515.
[40] N. W. Ashcroft, N. D. Mermin, *Solid State Physics*, Saunders, New York, USA **1976**.
[41] T.-C. Lee, O. A. Scherman, *Chem. Commun.* **2010**, *46*, 2438.